14

Quantized Mechanics of Nanotubes and Bundles

Nicola M. Pugno

Summary. In this chapter, the mechanics of carbon nanotubes and related bundles is reviewed, with an eye to their application as ultra-sharp tips for scanning probe "nanoscopy". In particular, the role of thermodynamically unavoidable, atomistic defects with different sizes and shapes on the fracture strength, fatigue life, and elasticity is quantified, thanks to new quantized fracture mechanics approaches. The reader is introduced in a simple way to such innovative treatments at the beginning of the chapter.

Key words: QFM, quantized, fracture, mechanics, strength, toughness, defect, nanotube, bundle, space elevator, scanning probe, microscopy

14.1 Introduction

Fabrication of carbon nanotubes (CNT) as nanoprobes in Scanning Probe Microscopy (SPM) dates back just to a decade ago [1, 2]; and today, the tremendous importance of such ultra-sharp tips is emerging (for a review see [3]). In the era of nanotechnology, "nanoscopy" techniques are, in fact, becoming more important as a consequence of their capability of exploring extremely small-scale phenomena. SPM is one of the most widely utilized microscopy techniques because it is a versatile tool for not only measuring the topology of surfaces but also manipulating the nanostructures. In spite of this, conventional silicon tips can easily break during an impact on the scanned surface and are not sufficiently slender to measure the topography of high-aspect ratio surfaces. In contrast, a CNT protruding from a conventional cantilever tip can be used as a strong ultra-sharp slender probe. If larger diameters are required, a nanotube bundle could replace the single nanotube. As the mechanical strength, elasticity, and slenderness of CNT and bundles are very high [4, 5], the CNT-probed "nanoscopy" brought a breakthrough in the development of a microscopy technique. However, defects can dramatically affect the mechanics of nanotubes and bundles, thus strongly limiting their performances.

In this chapter, the role of defects on the strength of nanotubes and bundles, based on new theoretical, deterministic, and statistical approaches of quantized fracture mechanics (QFM) proposed by the Author [6–9], is reviewed. The role of thermodynamically unavoidable, atomistic defects with different sizes and shapes is thus quantified on brittle fracture, fatigue, and elasticity, for nanotubes and bundles.

The chapter is organized in 12 short sections, as follows: Introduction is reported as the first section and Conclusions is reported as the last section; in Sect. 14.2, we review the QFM approaches; in Sect. 14.3, we apply them to calculate the fracture strength of nanotubes and bundles, containing defects with given sizes and shapes; whereas in Sect. 14.4, the impact strength is reported; in Sect. 14.5, elastic-plastic or hyper-elastic materials, rough cracks, and finite domains are treated; in Sect. 14.6, the fatigue life time is estimated; in Sect. 14.7, the Young's modulus degradation is quantified; in Sects. 14.8 and 14.9, we compare our results on strength and elasticity with atomistic simulations and nanotensile tests of CNT; in Sect. 14.10, we demonstrate that defects are thermodynamically unavoidable, evaluating the minimum defect size and the corresponding maximum achievable strength; in Sect. 14.11 , we calculate the strength of nanotube bundles by using hierarchical simulations and also discuss the related size effect.

14.2 Quantized Fracture Mechanics Approaches

According to the classical, continuum-based, Linear Elastic Fracture Mechanics (LEFM, [10]), the strength of a structure can be computed by Griffith's energy balance during a crack propagation or, equivalently, by setting the stress-intensity factor K equal to its critical value, the fracture toughness of the material K_{C}, i.e., $K = K_{\mathrm{C}}$. The stress-intensity factor K, for crack propagations – mode I (opening), mode II (sliding), or mode III (tearing), is only a function of the geometry and applied loads. On the other hand, if the hypothesis of the continuous crack advancement is relaxed, and thus a quantized energy balance is assumed [6], a more general (QFM, [7]) is formulated. The crack propagation will take place when

$$K^* = \sqrt{\langle K^2 \rangle_l^{l+\Delta l}} = K_{\mathrm{C}}; \text{ Modes I, II, III,} \tag{14.1}$$

where K^* is the square root of the mean value of the square of the stress-intensity factor along a fracture quantum Δl, for a crack of length l.

Analogously, for dynamic loads the "mean" value of the stress-intensity factor must be considered during the time quantum Δt, connected to the time $\Delta l \,/\, c$ – with c crack speed – to generate a fracture quantum. Accordingly, for Dynamic Quantized Fracture Mechanics (DQFM, [8]) the crack propagation will take place when

$$K_{\mathrm{d}}^{*} = \sqrt{\left\langle \langle K^2 \rangle_{l}^{l+\Delta l} \right\rangle_{t-\Delta t}^{t}} = K_{\mathrm{C}}; \text{Modes I, II, III.} \tag{14.2}$$

Equation (14.2), in analogy to Quantum Mechanics (QM) that is erected on the Planck's constant $\hbar$, is based on the existence of the action quantum $G_C \Delta l \Delta t$, where G_C is the fracture energy of the material ($G_{\mathrm{C}} = K_{\mathrm{C}}^2 / E$, where E is the Young's modulus).

Note that the classical, continuum-based, Dynamic Fracture Mechanics (DFM, [11]) would imply $K = K_{\mathrm{dC}}$, where K_{dC} is the a priori, unknown dynamic fracture initiation toughness, observed to be experimentally different from K_{C}, especially for severe loading rates, e.g., impacts. On the other hand, (14.2) reproduces very well the experimental observations on times to failure also for severe loading rates [8]. Thus, DQFM can treat severe loading rates, e.g., impacts, in contrast to DFM. DFM corresponds to the limit case of DQFM for $\Delta t \to 0$, and becomes not predictive for severe impacts, requiring an *ad hoc* dynamic, fracture initiation toughness. In the DQFM treatment, the dynamic, fracture initiation toughness is identical to its static value, as must physically be. Moreover, classical LEFM, which corresponds to the limit case of QFM with $\Delta l \to 0$, can be applied only to "large" and sharp cracks, i.e., to cracks having length larger than the fracture quantum and vanishing tip radius. In contrast, QFM has no restriction in treating defects with any size and shape.

Instead of a classical, continuum-based, maximum stress criterion, i.e., $\sigma_{\max} = \sigma_{\mathrm{C}}$, where $\sigma_{\max}$ is the maximum stress in the structure and σ_C is the strength of the material, the stress analog of QFM must be written as [12,13]

$$\sigma^{*} = \langle \sigma_{\mathrm{tip}} \rangle_{0}^{\Delta l} = \sigma_{\mathrm{C}} \text{ Mode I; for Modes II, III} : \sigma \to \tau, \tag{14.3}$$

where σ_{tip} is the opening – for mode I, stress at the tip of a defect, where is located the origin of the reference system; for modes II or III – the normal stress and strength must be evidently replaced by the corresponding shear stress τ and strength τ_C.

For dynamic loads this stress criterion has to be rewritten as [14]:

$$\sigma_{\mathrm{d}}^{*} = \left\langle \langle \sigma_{\mathrm{tip}} \rangle_{0}^{\Delta l} \right\rangle_{t-\Delta t}^{t} = \sigma_{\mathrm{C}} \text{ Mode I; for Modes II, III} : \sigma \to \tau, \tag{14.4}$$

representing the stress analog of DQFM.

Equations (14.1) and (14.2) are based on stress-intensity factors, whereas (14.3) and (14.4) on stress. However, note that considering, for example QFM, the free-parameter Δl can be fixed to reproduce for $l \to 0$ the classical criterion $\sigma_{\max} = \sigma_{\mathrm{C}}$: thus, QFM implies a smooth transition between the criteria of $\sigma_{\max} = \sigma_{\mathrm{C}}$ for vanishing crack length to $K = K_{\mathrm{C}}$ for large cracks (where $K^{*} \approx K$). Moreover, imposing that the criteria of (14.1) and (14.3) have to predict the same failure for each value of l corresponds to a mixed criterion [9,15]. The corresponding fracture quantum capable of ensuring such an equality for each value of l can be derived consequently: in this case, the fracture quantum $\Delta l\,(l)$ becomes, more than a material constant, a well-defined

material/structural parameter. In formulae,

$$K^* = K_{\mathrm{C}} \,\&\, \sigma^* = \sigma_{\mathrm{C}} \, \Delta l : \text{same predictions, Mode I; or } \sigma \to \tau \text{ for Modes II, III.} \tag{14.5}$$

We finally note that (14.1) and (14.3) have been successfully applied also for fatigue limit predictions [16]. The corresponding, fatigue limit criteria can be formally written considering the variations of Δ in front of the symbols, interpreting ΔK^* and $\Delta \sigma^*$ as the amplitude ranges of K^*, σ^* in a cycle, ΔK_{C} as the threshold value of the stress-intensity factor, and $\Delta \sigma_{\mathrm{C}}$ as the plain-specimen fatigue limit.

As suggested by (14.5), imposing the same strength and/or time to failure predictions from (14.2) and (14.4), a new dynamic mixed criterion, in which both fracture as well as time quanta are derived, to ensure the equality of such predictions, is formulated [9]:

$$K^*_{\mathrm{d}} = K_{\mathrm{C}} \,\&\, \sigma^*_{\mathrm{d}} = \sigma_{\mathrm{C}} \, \Delta l, \, \Delta t : \text{same predictions, Mode I; or } \sigma \to \tau \text{ for Modes II, III} \tag{14.6}$$

In addition, substituting the stress with the corresponding strain in (14.3) and (14.4), normal, ε, for mode I; or tangential, γ, for mode II and III;, a strain static

$$\varepsilon^* = \langle \varepsilon_{\mathrm{tip}} \rangle_0^{\Delta l} = \varepsilon_C \,\text{Mode I; for Modes II, III} : \varepsilon \to \gamma, \tag{14.7}$$

and dynamic criteria

$$\varepsilon^*_{\mathrm{d}} = \left\langle \langle \varepsilon_{\mathrm{tip}} \rangle_0^{\Delta l} \right\rangle_{t-\Delta t}^{t} = \varepsilon_{\mathrm{C}} \,\text{Mode I; for Modes II, III} : \varepsilon \to \gamma, \tag{14.8}$$

are derived [9].

The quantized criteria of (14.3–14.8) require in general the expression of the complete – and not only asymptotic – stress field around the tip of the defect, well-known only for the simplest cases. On the other hand, the criteria of (14.1) and (14.2) can be applied in a very simple way, by starting from the well-known solutions for the stress-intensity factors; for example, hundreds of static and dynamic solutions are reported in the classical Murakami's Handbook [17]. Obviously, the predictions of different criteria are not coincident, but always similar, representing the asymptotic matching between the two classical regimes.

We note that not only (14.1) and (14.3) but all the criteria (1–8) can be rewritten for fatigue limit predictions, formally introducing the variations Δ in front of the symbols. However, such criteria estimate the beginning of the fatigue crack growth but not its evolution. On the other hand, regarding the evolution of the fatigue crack, substituting the stress-intensity factor K with its "quantized" version K^* in the Paris' law – or in its classical extensions – a quantized Paris' law, which has to be applied to short cracks and small systems too, is formulated [9] as

$$\frac{\mathrm{d}l}{\mathrm{d}N} \approx A\,(\Delta K^*)^{\alpha}\,, \tag{14.9}$$

where N is the number of cycles, A and α are the Paris' constants, and ΔK^* is the amplitude range of the "quantized" stress-intensity factor in a cycle.

For very short cracks $K^* \propto \sigma$ and (14.9) resembles the classical Whöler's law, i.e., $N_{\mathrm{f}}\,(\Delta\sigma)^{\beta} = B$, with B, β constants and N_{f} life time. Note that, similarly to brittle fracture, the fracture quantum itself could be fixed in fatigue to derive from (14.9) and in the limit case of crack length tending to zero, the same Whöler's prediction for the life time N_f [18, 19]. On the other hand, for very large cracks ($K^* \approx K$) (14.9) becomes the classical Paris' law. Equation (14.9) is a stress-intensity factor-based, quantized criterion for a fatigue crack growth. The stress analog can be formulated substituting $\Delta\sigma$ with $\Delta\sigma^*$ in the classical Whöler's law, i.e. [9]

$$N_{\mathrm{f}}\,(\Delta\sigma^*)^{\beta} = B. \tag{14.10}$$

Equations (14.9) and (14.10) correspond in fatigue crack growth to (14.1) and (14.3) or (14.2) and (14.4) in static or dynamic fracture. Accordingly, starting from these two analogs, it is clear that all the analogs of (14.1–14.8) can be easily formulated for fatigue crack growth also; for example, the mixed criterion of (14.5), ensuring the same fatigue life prediction N_{f}, has to be written as [9]:

$$\frac{\mathrm{d}l}{\mathrm{d}N} \approx A\,(\Delta K^*)^{\alpha}\ \&\ N_{\mathrm{f}}\,(\Delta\sigma^*)^{\beta} = B\,\Delta l : \text{same predictions.} \tag{14.11}$$

Finally, also the Weibull [20] statistical theory for the strength of solids can be quantized [9]. According to Weibull, the probability of failure P_f of a specimen of volume V under uniaxial stress σ is given by $P_{\mathrm{f}} = 1 - \exp\left(-\frac{1}{V_0}\int (\sigma\,/\,\sigma_0)^m\,\mathrm{d}V\right)$, where V_0 is a reference volume and σ_0 and m are two constants. If stress intensifications are present, as in cracked structures, the Weibull's integral does not converge: this represents a limit of the classical Weibull's statistics and can automatically be removed if instead of σ its "quantized" version σ^* (or σ^*_{d}) is considered, as

$$P_{\mathrm{f}} = 1 - \exp\left(-\frac{1}{V_0}\int_V (\sigma^*\,/\,\sigma_0)^m\,\mathrm{d}V\right). \tag{14.12}$$

Thus, the quantized crack advancement removes a paradox and a new statistics is generated.

In general, we conclude emphasizing that our definition of K^* and σ^* (also in dynamics) allow one to "quantize" classical, well-known criteria, based on stress and/or on stress-intensity factor. More powerful quantized approaches will result and the classical ones will be automatically recovered for the limit case of vanishing quanta, as required by the "Corresponding Principle." These

new criteria are ideal to study small-scale objects, where the intrinsic material strength cannot be considered further as infinitely high, as in nanotubes. The applications to nanotubes and bundles are presented in the following sections of the chapter.

14.3 Fracture Strength

By considering QFM [6–9], the failure stress σ_N for a nanotube having an atomic size q (the "fracture quantum") and containing an elliptical hole of half-axes a, perpendicular to the applied load, or nanotube axis; and b can be determined including in the asymptotic solution [7] the contribution of the far-field stress. We accordingly derive [21]

$$\frac{\sigma_{\mathrm{N}}(a,b)}{\sigma_{\mathrm{N}}^{(\mathrm{theo})}} = \sqrt{\frac{1+2a/q\,(1+2a/b)^{-2}}{1+2a/q}}, \sigma_{\mathrm{N}}^{(\mathrm{theo})} = \frac{K_{\mathrm{IC}}}{\sqrt{q\pi/2}}, \tag{14.13}$$

where $\sigma_{\mathrm{N}}^{(\mathrm{theo})}$ is the theoretical (defect-free) nanotube strength ($\sim$100 GPa) and K_{IC} is the material fracture toughness. The self-interaction between the tips has been neglected here (i.e., $a << \pi R$, with R nanotube radius) and would further reduce the failure stress (finite domains are treated in Sect. 14.5).

Regarding the defect shape, for a sharp crack perpendicular to the applied load $a/q = \text{const}$ and $b/q \to 0$, thus $\sigma_{\mathrm{N}} \approx \sigma_{\mathrm{N}}^{(\mathrm{theo})}/\sqrt{1+2a/q}$, and for $a/q >> 1$, i.e., large cracks, $\sigma_N \approx K_{IC}/\sqrt{\pi a}$ in agreement with LEFM; note that LEFM can (1) only treat sharp cracks and (2) unreasonably predicts an infinite defect-free strength. On the other hand, for a crack parallel to the applied load $b/q = \text{const}$ and $a/q \to 0$ and thus, $\sigma_{\mathrm{N}} = \sigma_{\mathrm{N}}^{(\mathrm{theo})}$, as it must be. In addition, regarding the defect size, for self-similar and small holes $a/b = \text{const}$ and $a/q \to 0$ and coherently $\sigma_{\mathrm{N}} = \sigma_{\mathrm{N}}^{(\mathrm{theo})}$; furthermore, for self-similar and large holes $a/b = \text{const}$ and $a/q \to \infty$, and we deduce $\sigma_{\mathrm{N}} \approx \sigma_{\mathrm{N}}^{(\mathrm{theo})}/(1+2a/b)$ in agreement with the stress concentration posed by elasticity; but elasticity (coupled with a maximum stress criterion) unreasonably predicts (3) a strength independent from the hole size and (4) tending to zero for cracks. Note the extreme consistency of (14.13), that removing all the discussed limitations (1–4) represents the first law capable of describing in a unified manner all the size- and shape effects for the elliptical holes, including cracks as limit case [21]. In other words, (14.13) shows that the two classical strength predictions based on stress intensifications (LEFM) or concentrations (elasticity) are only reasonable for "large" defects; (14.13) unifies their results and extends its validity to "small" defects ("large" and "small" are here with respect to the fracture quantum). It shows that even a small defect can dramatically reduce the mechanical strength of a nanotube, e.g., limiting the applications of ultra-sharp, nanotube-based tips, even if, in this context,

more significant are the impact strength and fatigue life of the nanotube tip, treated in Sects. 14.4 and 14.6, respectively.

For a nanotube bundle, an upperbound of the strength can be derived assuming the simultaneous failure of all the defective nanotubes present in the bundle. Accordingly, imposing the critical force equilibrium (mean-field approach) for a cable composed by nanotubes in numerical fractions f_{ab}, containing holes of half-axes a and b, we find the cable strength σ_{C} (ideal if $\sigma_{\mathrm{C}}^{(\mathrm{theo})}$) in the following form [21]:

$$\frac{\sigma_{\mathrm{C}}}{\sigma_{\mathrm{C}}^{(\mathrm{theo})}} = \sum_{a,b} f_{ab} \frac{\sigma_{\mathrm{N}}(a,b)}{\sigma_{\mathrm{N}}^{(\mathrm{theo})}}. \tag{14.14}$$

The summation is extended to all the different holes; the numerical fraction f_{00} of nanotubes is defect-free and $\sum_{a,b} f_{ab} = 1$. If all the defective nanotubes in the bundle contain identical holes $f_{ab} = f = 1 - f_{00}$ and $1 - \sigma_{\mathrm{C}} / \sigma_{\mathrm{C}}^{(\mathrm{theo})} = f\,(1 - \sigma_{\mathrm{N}} / \sigma_{\mathrm{N}}(\mathrm{theo}))$.

14.4 Impact Strength

Let us consider the simplest case of a semi-infinite crack in an otherwise unbounded body. The body is initially stress-free and at rest. At time $t = 0$ a pressure σ begins to act on the crack faces. In this case, as it is well-known, $K_I(t) = 2\sigma \frac{\sqrt{c_D t(1-2\nu)/\pi}}{(1-\nu)}$ [11], where c_{D} is the dilatational wave speed of the material and ν is its Poisson's ratio. Applying (14.2) we find the failure for a given time $t_f > \Delta t$, satisfying [9]

$$K_{\mathrm{I}}(t) = \frac{K_{\mathrm{IC}}}{\sqrt{1 - \Delta t / (2t_f)}} \equiv K_{\mathrm{dIC}}. \tag{14.15}$$

Thus, if classical DFM [11] is applied, i.e., $K_{\mathrm{I}}(t) = K_{\mathrm{dIC}}$, the "measured" fracture initiation toughness K_{dIC} will be observed, according to DQFM, time to failure dependent. In addition, note that, according to our time quantization, a minimum time to failure exists and it must be of the order of $t_{f\,\min} \approx \Delta t$. Considering very severe impacts ($t_f \to t_{f\,\min} \approx \Delta t$), the dynamic strength ($\propto K_{\mathrm{dIC}}$) is expected for this scheme $\sqrt{2}$ times larger than its static value ($\propto K_{\mathrm{IC}}$). For an applied pressure linearly increasing with time, the factor $\sqrt{2}$ is replaced by the factor 2 [8]. For different schemes a slightly different factor is expected. Roughly speaking, we could call this effect as the "doubling" of the impact strength (with respect to its static value). This is a well-known, experimental phenomenon [8] and is thus expected for nanotubes also.

14.5 Hyper-Elasticity, Elastic-Plasticity, Fractal Cracks, and Finite Domains

Equation (14.13) is based on linear elasticity, i.e., on a linear relationship $\sigma \propto \varepsilon$ between stress σ and strain ε. In contrast, let us assume $\sigma \propto \varepsilon^{\kappa}$, where $\kappa > 1$ denotes hyper-elasticity, as well as $\kappa < 1$ denotes elastic-plasticity. The power of the stress-singularity will accordingly be modified [22] from the classical value $1/2$ to $\alpha = \kappa/(\kappa+1)$. Thus, the problem is mathematically equivalent to that of a re-entrant corner [23], and consequently we predict

$$\frac{\sigma_{\mathrm{N}}(a,b,\alpha)}{\sigma_{\mathrm{N}}^{(\mathrm{theo})}} = \left(\frac{\sigma_{\mathrm{N}}(a,b)}{\sigma_{\mathrm{N}}^{(\mathrm{theo})}}\right)^{2\alpha}, \alpha = \frac{\kappa}{\kappa+1}. \tag{14.16}$$

A crack with a self-similar roughness, mathematically described by a fractal with non-integer dimension $1 < D < 2$, would similarly modify the stress-singularity, according to [24] $\alpha = (2-D)/2$; thus, with (14.16), we can also estimate the role of the crack roughness. Both plasticity and roughness reduce the severity of the defect, whereas hyper-elasticity enlarges its effect. For example, for a crack composed by n adjacent vacancies, we deduce $\sigma_{\mathrm{N}} / \sigma_{\mathrm{N}}^{(\mathrm{theo})} \approx (1+n)^{-\alpha}$. However, note that among these three effects only elastic-plasticity may have a significant role in CNT; in spite of this, fractal cracks could play an important role in nanotube bundles as a consequence of their larger size-scale, which would allow the development of a crack surface roughness. Hyper-elasticity is not expected to be relevant in this context.

Equation (14.13) does not consider the defect–boundary interaction. A graphene sheet having a finite width $2W$ can be treated by applying QFM starting from the related expression of the stress-intensity factor. However, to have an idea of the defect–boundary interaction, we can couple (14.13) with an approximated method [21], deriving the following correction $\sigma_{\mathrm{N}}(a,b,W) \approx C(W)\,\sigma_{\mathrm{N}}(a,b)$, $C(W) \approx (1-a/W) / \left(\sigma_{\mathrm{N}}(a,b)\,|_{q\to W-a} / \sigma_{\mathrm{N}}(\mathrm{theo})\right)$ (note that such a correction is valid also for $W \approx a$, whereas for $W >> a$ it becomes $C(W >> a) \approx 1 - a/W$). Similarly, the role of the defect orientation β could be treated by QFM considering the related, stress-intensity factor; roughly, one could use in (14.13) the self-consistent approximation $\sigma_{\mathrm{N}}(a,b,\beta) \approx \sigma_{\mathrm{N}}(a,b)\cos^2\beta + \sigma_{\mathrm{N}}(b,a)\sin^2\beta$.

14.6 Fatigue Life

The SPM nanotube tip is cyclically loaded during surface scanning, thus fatigue plays a major role. By integrating the quantized Paris' law of (14.9), we derive the following number of cycles to failure, or life time [21]:

$$\frac{N_{\mathrm{N}}(a)}{N_{\mathrm{N}}^{(\mathrm{theo})}} = \frac{(1+q/W)^{1-m/2} - (a/W+q/W)^{1-m/2}}{(1+q/W)^{1-m/2} - (q/W)^{1-m/2}},\ m \neq 2 \tag{14.17a}$$

and

$$\frac{N_{\mathrm{N}}(a)}{N_{\mathrm{N}}^{(\mathrm{theo})}} = \frac{\ln\{(1+q/W)/(a/W+q/W)\}}{\ln\{(1+q/W)/(q/W)\}}, m=2 \tag{14.17b}$$

where $m > 0$ is the material Paris' exponent. Note that according to Wöhler $N_{\mathrm{N}}^{(\mathrm{theo})} = K\Delta\sigma^{-k}$, where K and k are material constants and $\Delta\sigma$ is the amplitude of the stress range during the oscillations.

Only defects remaining self-similar during fatigue growth have to be considered, thus only a crack (of half-length a) is of interest in this context. By means of (14.17) the time to failure can be estimated, similarly to the brittle fracture treated by (14.13).

For a bundle, considering a mean-field approach (similarly to (14.14)) yields:

$$\frac{N_{\mathrm{C}}}{N_{\mathrm{C}}^{(\mathrm{theo})}} = \sum_a f_a \frac{N_{\mathrm{N}}(a)}{N_{\mathrm{N}}^{(\mathrm{theo})}}. \tag{14.18}$$

Better predictions could be derived integrating the quantized Paris' law for a finite width strip. However, we note that the role of the finite width is already included in (14.17), even if these are rigorously valid in the limit of W tending to infinity.

14.7 Elasticity

Consider a nanotube of lateral surface A under tension and containing a transversal crack of half-length a. Interpreting the incremental compliance, due to the presence of the crack, as a Young's modulus (here denoted by E) degradation we find $\frac{E(a)}{E^{(\mathrm{theo})}} = 1 - 2\pi\frac{a^2}{A}$ [25]. Thus, recursively, considering Q cracks having sizes a_i or, equivalently, M different cracks with multiplicity Q_i ($Q = \sum_{i=1}^{M} Q_i$), noting that $n_i = \frac{2a_i}{q}$ represents the number of adjacent vacancies in a crack of half-length a_i, with q atomic size, and $v_i = \frac{Q_i n_i}{A/q^2}$ its related numerical (or volumetric) vacancy fraction, we find [25]:

$$\frac{E}{E^{(\mathrm{theo})}} = \prod_{i=1}^{Q} \frac{E(a_i)}{E^{(\mathrm{theo})}} \approx 1 - \xi \sum_{i=1}^{M} v_i n_i, \tag{14.19}$$

with $\xi \geq \pi/2$, where the equality holds for isolated cracks. Equation (14.19) can be applied to nanotubes or nanotube bundles containing defects in volumetric percentages v_i.

Forcing the interpretation of our formalism, we note that $n_i = 1$ would describe a single vacancy, i.e., a small hole. Thus, as a first approximation, different defect geometries, from cracks to circular holes, e.g., elliptical holes,

could in principle be treated by (14.19); we have to interpret n_i as the ratio between the transversal and longitudinal (parallel to the load) defect sizes ($n_i = a_i \,/\, b_i$). Introducing the i-th defect eccentricity e_i as the ratio between the lengths of the longer and shorter axes, as a first approximation $n_i\,(\beta_i) \approx e_i \cos^2\beta_i + 1 \,/\, e_i \sin^2\beta_i$, where β_i is the defect orientation. For a single defect typology $\frac{E}{E^{(theo)}} \approx 1 - \xi v n$, in contrast to the common assumption $\frac{E}{E^{(\mathrm{theo})}} \approx 1 - v$, rigorously valid only for the material density, for which $\frac{\rho_C}{\rho_C^{(theo)}} \equiv 1 - v$. Note that the failure strain for a defective nanotube or nanotube bundle can also be predicted, by $\varepsilon_{\mathrm{N,C}} \,/\, \varepsilon_{\mathrm{N,C}}^{(\mathrm{theo})} = \left(\sigma_{\mathrm{N,C}} \,/\, \sigma_{\mathrm{N,C}}^{(\mathrm{theo})}\right) / \left(E \,/\, E^{(\mathrm{theo})}\right)$.

In contrast to what happens for fracture and fatigue, defects affect the elasticity in a significant but not dramatic way.

14.8 Atomistic Simulations

Let us study the influence on the strength of nano-cracks and circular nano-holes. n atomic adjacent vacancies perpendicular to the load, correspond to a blunt nano-crack of length $2a \approx nq$ and thickness $2b \approx q$ (or $2a \approx nq$ with a radius at tips of $b^2 \,/\, a \approx q \,/\, 2$). Similarly, nano-holes of size m can be considered: the index $m = 1$ corresponds to the removal of an entire hexagonal ring, $m = 2$ to the additional removal of the six hexagons around the former one (i.e. the adjacent perimeter of 18 atoms), $m = 3$ to the additional removal of the neighbouring 12 hexagonal rings (next adjacent perimeter), and so on (thus $a = b \approx q(2m-1) \,/\, \sqrt{3}$) [7]. QM, semi-empirical (PM3 method), Molecular Mechanics (MM; with a modified Tersoff-Brenner potential of second generation (MTB-G2) or a modified Morse potential (M)) and coupled QM/MM calculations [26–30] are reported and extensively compared in Table 14.1 with the QFM predictions of (14.13) [7, 21]. The comparison shows a relevant agreement, confirming and demonstrating that just a few vacancies can dramatically reduce the strength of a single nanotube or of a nanotube bundle as described by (14.14) that predicts for $f \approx 1$, $\sigma_{\mathrm{C}} \,/\, \sigma_{\mathrm{C}}^{(\mathrm{theo})} \approx \sigma_{\mathrm{N}} \,/\, \sigma_{\mathrm{N}}^{(\mathrm{theo})}$. For example, assuming large holes ($m \to \infty$) and applying QFM to a defective bundle ($f \approx 1$), we predict $1 - \sigma_{\mathrm{C}} \,/\, \sigma_{\mathrm{C}}^{(\mathrm{theo})} \approx 1 - \sigma_{\mathrm{N}} \,/\, \sigma_{\mathrm{N}}^{(\mathrm{theo})} \approx 67\%$.

Note that an elastic ($\kappa \approx 1$) nearly perfectly plastic ($\kappa \approx 0$) behaviour, with a flow stress at ∼30–35GPa for strains larger than ∼3–5%, has been recently observed in tensile tests of CNT [31], globally suggesting $\kappa \approx 0.6-0.7$; similarly, numerically computed stress-strain curves [32] reveal for an armchair (5,5) carbon nanotube $\kappa \approx 0.8$, whereas for a zig-zag (9,0) nanotube $\kappa \approx 0.7$, suggesting that the plastic correction reported in Sect. 14.5 could have a role.

Regarding elasticity, we note that (14.19) [25] can be viewed as a generalization of the approach proposed in [33] considering three different types of defects.

Table 14.1. Atomistic simulations [26–29] vs. QFM predictions, for nano-cracks of size n or nano-holes of size m

Nanotube Type	Nanocrack (n) and nanohole (m) sizes	Strength [GPa] by QM (MTB-G2) and MM (PM3; M) QM/MM atomistic or QFM calculations
[5,5]	Defect-free	105 (MTB-G2); 135 (PM3)
[5,5]	$n = 1$(sym. + H)	85 (MTB-G2), 79 (QFM); 106 (PM3), 101 (QFM)
[5,5]	$n = 1$(Asym. + H)	71 (MTB-G2), 79 (QFM); 99 (PM3), 101 (QFM)
[5,5]	$n = 1$(Asym.)	70 (MTB-G2), 79 (QFM); 100 (PM3), 101 (QFM)
[5,5]	$n = 2$(Sym.)	71 (MTB-G2), 63 (QFM); 105 (PM3), 81 (QFM)
[5,5]	$n = 2$(Asym.)	73 (MTB-G2), 63 (QFM); 111 (PM3), 81 (QFM)
[5,5]	$m = 1$(+H)	70 (MTB-G2), 68 for long tube, 79 (QFM); 101 (PM3), 101 (QFM)
[5,5]	$m = 2$(+H)	53 (MTB-G2), 50 for long tube, 67 (QFM); 78 (PM3), 86 (QFM)
[10,10]	Defect-free	88 (MTB-G2); 124 (PM3)
[10,10]	$n = 1$(sym. + H)	65 (MTB-G2), 66 (QFM)
[10,10]	$n = 1$(Asym. + H)	68 (MTB-G2), 66 (QFM)
[10,10]	$n = 1$(Sym.)	65 (MTB-G2), 66 (QFM); 101 (PM3), 93 (QFM)
[10,10]	$n = 2$(Sym.)	64 (MTB-G2), 53 (QFM); 107 (PM3), 74 (QFM)
[10,10]	$n = 2$(Asym.)	65 (MTB-G2), 53 (QFM); 92 (PM3), 74 (QFM)
[10,10]	$m = 1$(+H)	56 (MTB-G2), 52 for long tube, 66 (QFM); 89 (PM3), 93 (QFM)
[10,10]	$m = 2$(+H)	42 (MTB-G2), 36 for long tube, 56 (QFM); 67 (PM3), 79 (QFM)
[50,0]	Defect-free	89 (MTB-G2)
[50,0]	$m = 1$(+H)	58 (MTB-G2); 67 (QFM)
[50,0]	$m = 2$(+H)	46 (MTB-G2); 57 (QFM)
[50,0]	$m = 3$(+H)	40 (MTB-G2); 44 (QFM)
[50,0]	$m = 4$(+H)	36 (MTB-G2); 41 (QFM)
[50,0]	$m = 5$(+H)	33 (MTB-G2); 39 (QFM)
[50,0]	$m = 6$(+H)	31 (MTB-G2); 37 (QFM)
[100,0]	Defect-free	89 (MTB-G2)
[100,0]	$m = 1$(+H)	58 (MTB-G2); 67 (QFM)
[100,0]	$m = 2$(+H)	47 (MTB-G2); 57 (QFM)
[100,0]	$m = 3$(+H)	42 (MTB-G2); 44 (QFM)
[100,0]	$m = 4$(+H)	39 (MTB-G2); 41 (QFM)
[100,0]	$m = 5$(+H)	37 (MTB-G2); 39 (QFM)
[100,0]	$m = 6$(+H)	35 (MTB-G2); 37 (QFM)
[29,29]	Defect-free	101 (MTB-G2)
[29,29]	$m = 1$(+H)	77 (MTB-G2); 76 (QFM)
[29,29]	$m = 2$(+H)	62 (MTB-G2); 65 (QFM)
[29,29]	$m = 3$(+H)	54 (MTB-G2); 50 (QFM)
[29,29]	$m = 4$(+H)	48 (MTB-G2); 46 (QFM)
[29,29]	$m = 5$(+H)	45 (MTB-G2); 44 (QFM)
[29,29]	$m = 6$(+H)	42 (MTB-G2); 42 (QFM)

(*Continued*)

Table 14.1. (Continued)

Nanotube Type	Nanocrack (n) and nanohole (m) sizes	Strength [GPa] by QM (MTB-G2) and MM (PM3; M) QM/MM atomistic or QFM calculations
[47,5]	Defect-free	89 (MTB-G2)
[47,5]	$m = 1$(+H)	57 (MTB-G2); 67 (QFM)
[44,10]	Defect-free	89 (MTB-G2)
[44,10]	$m = 1$(+H)	58 (MTB-G2); 67 (QFM)
[40,16]	Defect-free	92 (MTB-G2)
[40,16]	$m = 1$(+H)	59 (MTB-G2); 69 (QFM)
[36,21]	Defect-free	96 (MTB-G2)
[36,21]	$m = 1$(+H)	63 (MTB-G2); 72 (QFM)
[33,24]	Defect-free	99 (MTB-G2)
[33,24]	$m = 1$(+H)	67 (MTB-G2); 74 (QFM)
[80, 0]	Defect-free	93 (M)
[80, 0]	$n = 2$	64 (M); 56 (QFM)
[80, 0]	$n = 4$	50 (M); 43 (QFM)
[80, 0]	$n = 6$	42 (M); 35 (QFM)
[80, 0]	$n = 8$	37 (M); 32 (QFM)
[40, 0] (nested by a [32, 0])	Defect-free	99 (M)
[40, 0] (nested by a [32, 0])	$n = 2$	73 (M); 69 (QFM + vdW interaction ∼10GPa)
[40, 0] (nested by a [32, 0])	$n = 4$	57 (M); 56 (QFM + vdW interaction ∼10GPa)
[40, 0] (nested by a [32, 0])	$n = 6$	50 (M); 48 (QFM + vdW interaction ∼10GPa)
[40, 0] (nested by a [32, 0])	$n = 8$	44 (M); 44 (QFM + vdW interaction ∼10GPa)
[100,0]	Defect-free	89 (MTB-G2)
[100,0]	$n = 4$	50 (M); 41 (QFM)
[10,0]	Defect free	124 (QM); 88 (MM);
[10,0]	$N = 1$	101 (QM) 95 (QM/MM) 93 (QFM); 65 (MM) 66 (QFM)

The QFM predictions are here obtained simply considering in (14.13) $2a \,/\, q = n$, $2b \,/\, q = 1$ for cracks of size n or $a \,/\, q = b \,/\, q = (2m-1) \,/\, \sqrt{3}$ for holes of size m. Quantum mechanics (QM) semi-empirical calculations (PM3 method), Molecular Mechanics (MM) calculations (modified Tersoff-Brenner potential of second generation (MTB-G2), modified Morse potential (M)) and coupled QM/MM calculations. The symbol (+H) means that the defect was saturated with hydrogen. Symmetric and asymmetric bond reconstructions were also considered; the tubes are "short", if not otherwise specified. We have roughly ignored in the QFM predictions the difference between symmetric and asymmetric bond reconstruction, hydrogen saturation and length effect (for shorter tubes an increment in the strength is always observed, as an intrinsic size effect), noting that the main differences in the atomistic simulations are imputable to the used potential. For nested nanotubes a strength increment of ∼10 GPa is here assumed to roughly take into account the van der Walls (vdW) interaction between the walls

14.9 Nanotensile Tests

The discussed tremendous defect sensitivity, described by (14.13), is confirmed by a statistical analysis based on Nanoscale Weibull Statistics (NWS, [34]) applied to the nanotensile tests. According to this treatment, the probability of failure P for a nearly defect-free nanotube under a tensile stress σ_N is independent from its volume (or surface), in contrast to classical Weibull Statistics [20], namely:

$$P = 1 - \exp -N_{\mathrm{N}} \left(\frac{\sigma_{\mathrm{N}}}{\sigma_0} \right)^w , \tag{14.20}$$

where w is the nanoscale Weibull modulus, σ_0 is the nominal failure stress (i.e. corresponding to a probability of failure of 63%) and $N_{\mathrm{N}} \equiv 1$. In classical Weibull statistics $N_N \equiv V/V_0$ for volume dominating defects (or $N_{\mathrm{N}} = A/A_0$ for surface dominating defects), i.e., N_N is the ratio between the volume (or surface) of the structure and a reference volume (or surface). The experimental data on CNT [4, 5] were treated [34] according to nanoscale and classical Weibull statistics, Fig. 14.1: the coefficients of correlation were found to be much higher for the nanoscale statistics than for the classical one (0.93 against 0.67, $w \approx 2.7$ and $\sigma_0 \approx 31 - 34\,\mathrm{GPa}$). Other data set on multi walled CNT tensile experiments [31, 35] are also treated in Fig. 14.1 [21].

Note that volume- or surface-based Weibull statistics are identical in treating the external wall of the tested nanotubes, just an atomic layer thick.

All these experimental data [4,5,31,35] are treated in Table 14.2, by applying QFM in the form of (14.13): non-linear multiple solutions for identifying

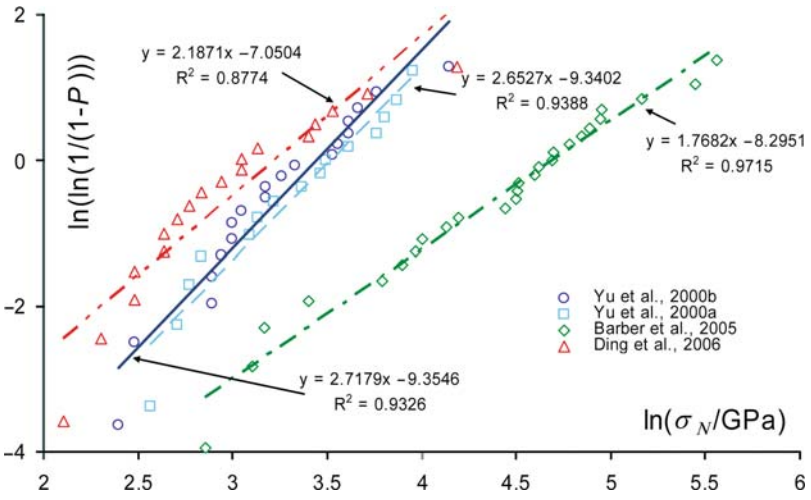

Fig. 14.1. Nanoscale Weibull Statistics, *straight lines*, applied to the new nanotensile experiments on carbon nanotubes

Table 14.2. Experiments vs. QFM predictions; strength reduction $\sigma_{\mathrm{N}}(a,b)$ / $\sigma_{\mathrm{N}}^{(\mathrm{theo})}$ derived according to (14.13)

σ_{N} / $\sigma_{\mathrm{N}}^{(\mathrm{theo})}$ $2a/q$ 2 b/q	**0**	**1**	**2**	**3**	**4**	**5**	**6**	**7**	**8**	**9**	**10**	**∞**
0	1.00*	1.00*	1.00*	1.00*	1.00*	1.00*	1.00*	1.00*	1.00*	1.00*	1.00*	1.00
1	0.71*	0.75	0.79	0.82	0.85	0.87*	0.88*	0.90	0.91	0.91	0.92	1.00
2	0.58	0.60*	0.64*	0.68	0.71*	0.73	0.76	0.78*	0.79	0.81	0.82	1.00
3	0.50	**0.52**	0.54*	0.58	0.61	0.64*	0.66*	0.68	0.70*	0.72	0.74	1.00
4	**0.45**	0.46	**0.48**	0.51*	0.54*	0.56	0.59	0.61	*0.63*	0.65	0.67	1.00
5	0.41	0.42	0.44*	0.46	0.48	0.51*	0.53*	0.55*	0.58	0.59	0.61	1.00
6	0.38	0.38	0.40	0.42	0.44*	0.47	0.49*	0.51*	0.53*	0.55*	0.57	1.00
7	*0.35*	0.36	***0.37***	*0.39*	0.41	***0.43***	**0.45**	0.47	0.49*	0.51*	0.53*	1.00
8	**0.33**	*0.34*	*0.35*	***0.37***	0.38	0.40	0.42	0.44*	0.46	**0.48**	0.49*	1.00
9	**0.32**	**0.32**	**0.33**	*0.34*	0.36	0.38	0.40	0.41	***0.43***	**0.45**	0.46	1.00
10	0.30*	0.30*	0.31	**0.33**	*0.34*	0.36	***0.37***	*0.39*	0.41	0.42	0.44*	1.00
11	**0.29**	**0.29**	0.30*	0.31	**0.32**	*0.34*	*0.35*	***0.37***	*0.39*	0.40	0.42	1.00
12	*0.28*	*0.28*	**0.29**	0.30*	0.31	**0.32**	*0.34*	*0.35*	***0.37***	0.38	0.40	1.00
13	0.27	0.27	*0.28*	**0.29**	0.30*	0.31	**0.32**	*0.34*	*0.35*	0.36	0.38	1.00
14	*0.26*	*0.26*	0.27	0.27	**0.29**	0.30*	0.31	**0.32**	*0.34*	*0.35*	0.36	1.00
15	**0.25**	**0.25**	*0.26*	0.27	0.27	**0.29**	0.30*	0.31	**0.32**	*0.34*	*0.35*	1.00
16	0.24*	0.24*	**0.25**	*0.26*	0.27	*0.28*	**0.29**	0.30*	0.31	0.32	**0.33**	1.00
17	0.24*	0.24*	0.24*	**0.25**	*0.26*	0.27	*0.28*	**0.29**	0.30*	0.31	**0.32**	1.00
18	**0.23**	**0.23**	0.24*	0.24*	**0.25**	*0.26*	0.27	*0.28*	**0.29**	0.30*	0.31	1.00
19	**0.22***	**0.22***	**0.23**	**0.23**	0.24*	0.25	*0.26*	0.27	*0.28*	**0.29**	0.30*	1.00
20	**0.22***	**0.22***	**0.22***	**0.23**	0.24*	0.24*	**0.25**	0.26	0.27	0.28	**0.29**	1.00
21	*0.21*	*0.21*	**0.22***	**0.22***	**0.23**	0.24*	**0.25**	**0.25**	*0.26*	0.27	*0.28*	1.00
22	*0.21*	*0.21*	*0.21*	**0.22***	**0.22***	**0.23**	0.24*	**0.25**	*0.26*	0.27	*0.28*	1.00
23	*0.20*	*0.21*	*0.21*	*0.21*	**0.22***	**0.23**	**0.23**	0.24*	**0.25**	*0.26*	0.27	1.00
24	*0.20*	*0.20*	*0.20*	*0.21*	*0.21*	**0.22***	**0.23**	0.24*	0.24*	**0.25**	*0.26*	1.00
25	*0.20*	*0.20*	*0.20*	*0.20*	*0.21*	**0.22***	**0.22***	**0.23**	0.24*	**0.25**	*0.26*	1.00
26	*0.19*	*0.19*	*0.20*	*0.20*	*0.20*	*0.21*	**0.22***	**0.22***	**0.23**	0.24*	**0.25**	1.00
27	*0.19*	*0.19*	*0.19*	*0.20*	*0.20*	*0.21*	*0.21*	**0.22***	**0.23**	0.24*	0.24*	1.00
28	*0.19*	*0.19*	*0.19*	*0.19*	*0.20*	*0.20*	*0.21*	**0.22***	**0.22***	**0.23**	0.24*	1.00
29	*0.18*	*0.18*	*0.19*	*0.19*	*0.19*	*0.20*	*0.20*	*0.21*	**0.22***	**0.23**	**0.23**	1.00
30	*0.18*	*0.18*	*0.18*	*0.19*	*0.19*	*0.19*	*0.20*	*0.21*	*0.21*	**0.22***	**0.23**	1.00
31	*0.18*	*0.18*	*0.18*	*0.18*	*0.19*	*0.19*	*0.20*	*0.20*	*0.21*	**0.22***	**0.22***	1.00
32	**0.17***	**0.17***	*0.18*	*0.18*	*0.18*	*0.19*	*0.19*	*0.20*	*0.21*	*0.21*	**0.22***	1.00
33	**0.17***	**0.17***	**0.17***	*0.18*	*0.18*	*0.19*	*0.19*	*0.20*	*0.20*	*0.21*	*0.21*	1.00
34	**0.17***	**0.17***	**0.17***	**0.17***	*0.18*	*0.18*	*0.19*	*0.19*	*0.20*	*0.20*	*0.21*	1.00
35	**0.17***	**0.17***	**0.17***	**0.17***	**0.17***	*0.18*	*0.18*	*0.19*	*0.19*	*0.20*	*0.21*	1.00
36	**0.16**	**0.16**	**0.17***	**0.17***	**0.17***	*0.18*	*0.18*	*0.19*	*0.19*	*0.20*	*0.20*	1.00
37	**0.16**	**0.16**	**0.16**	**0.17***	**0.17***	**0.17***	*0.18*	*0.18*	*0.19*	*0.19*	*0.20*	1.00
38	**0.16**	**0.16**	**0.16**	**0.16**	**0.17***	**0.17***	*0.18*	*0.18*	*0.19*	*0.19*	*0.20*	1.00
39	**0.16**	**0.16**	**0.16**	**0.16**	**0.17***	**0.17***	**0.17***	*0.18*	*0.18*	*0.19*	*0.19*	1.00
40	**0.16**	**0.16**	**0.16**	**0.16**	**0.16**	**0.17***	**0.17***	*0.18*	*0.18*	*0.19*	*0.19*	1.00
41	**0.15**	**0.15**	**0.16**	**0.16**	**0.16**	**0.16**	**0.17***	**0.17***	*0.18*	*0.18*	*0.19*	1.00
42	**0.15**	**0.15**	**0.15**	**0.16**	**0.16**	**0.16**	**0.17***	**0.17***	*0.18*	*0.18*	*0.19*	1.00
43	**0.15**	**0.15**	**0.15**	**0.15**	**0.16**	**0.16**	**0.16**	**0.17***	**0.17***	*0.18*	*0.18*	1.00
44	**0.15**	**0.15**	**0.15**	**0.15**	**0.16**	**0.16**	**0.16**	**0.17***	**0.17***	*0.18*	*0.18*	1.00
45	**0.15**	**0.15**	**0.15**	**0.15**	**0.15**	**0.16**	**0.16**	**0.16**	**0.17***	**0.17***	*0.18*	1.00

(*Continued*)

Table 14.2. (Continued)

46	**0.15**	**0.15**	**0.15**	**0.15**	**0.15**	**0.15**	**0.16**	**0.16**	**0.17***	**0.17***	*0.18*	1.00
47	0.14	0.14	**0.15**	**0.15**	**0.15**	**0.15**	**0.16**	**0.16**	**0.16**	**0.17***	**0.17***	1.00
48	0.14	0.14	0.14	**0.15**	**0.15**	**0.15**	**0.15**	**0.16**	**0.16**	**0.17***	**0.17***	1.00
49	0.14	0.14	0.14	0.14	**0.15**	**0.15**	**0.15**	**0.16**	**0.16**	**0.16**	**0.17***	1.00
50	0.14	0.14	0.14	0.14	**0.15**	**0.15**	**0.15**	**0.15**	**0.16**	**0.16**	**0.17***	1.00
∞	0.00	0.00	0.00	0.00	0.00	0.00	0.00	0.00	0.00	0.00	0.00	$(1+2a/b)^{-1}$

In **bold** type are represented the 15 different nanostrengths measured on single walled CNT in bundle [4]; whereas in *italic* we report the 19 nanostrengths measured on multi walled CNT[5], and in underlined type the most recent 18 observations [31]. All the data are reported with the exception of the five smallest values of 0.08, 0.10 [31], 0.11 [5], 0.12 [5,31] and 0.13 [4], for which we would need for example adjacent vacancies ($2b/q{\sim}1$) in number $n = 2a/q =$ 138–176, 90–109, 75–89, 64–74 and 55–63 respectively. The 26 strengths measured in [35] are also treated (*asterisks*), simply assuming two interacting walls for $100 < \sigma_N^{(\exp)} \leq 200$ gigapascals (thus $\sigma_N = \sigma_N^{(\exp)} / 2$) or 3 interacting walls for $200 < \sigma_N^{(\exp)} \leq 300$ gigapascals ($\sigma_N = \sigma_N^{(\exp)} / 3$). All the experiments are referred to $\sigma_N^{(theo)} = 100$GPa ($q{\sim}0.25$ nm). If all the nanotubes in the cable contain identical holes, $\sigma_C / \sigma_C^{(theo)} = \sigma_N / \sigma_N^{(theo)}$

the defects corresponding to the measured strength clearly emerge; however these are quantifiable, showing that a small defect is sufficient to rationalize the majority of the observed strong strength reductions.

Finally, the anomalous (due to plasticity) experimental results [31] are differently treated in Table 14.3, with respect to both strength and elasticity, assuming the presence of transversal nanocracks. The ideal strength is assumed to be of 100GPa and the theoretical Young's modulus of 1.3 TPa; by (14.13) the crack length n is calculated and introduced in (14.19) to derive the related vacancy fraction v ($\xi = \pi / 2$).

Fracture in two cases was observed at the clamp; in one case the clamp itself failed, thus the deduced strength represents a lower bound of the nanotube strength. Three nanotubes were multiple loaded (in two a,b and A,B or in three I,II,III steps), i.e., after the breaking in two pieces of a nanotube, one of the two pieces was again tested and fractured at a higher stress. Two nanotubes displayed a plastic flow.

A vacancy fraction of the order of few ‰ is estimated, suggesting that such nanotubes are much more defective than as imposed by the thermodynamic equilibrium, even if the defects are small and isolated. However, note that other interpretations are still possible, e.g., assuming the nanotube is coated by an oxide layer and rationalizing the ratio between the observed Young's modulus and its theoretical value as the volumetric fraction (for softer coating layers) of carbon in the composite structure.

Table 14.3. The experiments [31] are here treated with respect to both strength and elasticity, assuming the presence of transversal nanocracks composed by n adjacent vacancies

MWCNT number and fracture typology	Strength [GPa]	Young's modulus [GPa]	κ	n	$v\%$
1 (multiple load A)	8.2	1,100	1.01	148	0.07
2 (clamp failed)	10	840	0.98	100	0.23
3	12	680	1.00	69	0.44
4 (failure at the clamp)	12	730	0.98	69	0.40
5 (multiple load B)	14	1,150	1.02	51	0.14
6 (multiple load a)	14	650	0.97	51	0.62
7	15	1,200	1.05	44	0.11
8	16	1,200	1.02	39	0.13
9	17	960	1.00	34	0.49
10	19	890	0.97	27	0.74
11 (multiple load b)	21	620	0.99	22	1.51
12 (multiple load I)	21	1,200	0.99	22	0.22
13 (multiple load II)	23	1,250	0.99	18	0.17
14	30	870	1.00	11	1.92
15 (plasticity observed)	31	1,200	0.59 (0.99)	10	0.49
16 (plasticity observed)	34	680	0.69 (1.02)	8	3.80
17 (multiple load III)	41	1,230	1.03	5	0.69
18 (failure at the clamp)	66	1,100	0.98	2	4.90

The constitutive parameter κ has been estimated as $\kappa \approx \ln(\varepsilon_N)/\ln(\sigma_N/E)$ for all the tests: note the low values for the two nanotubes that revealed plasticity (in brackets the values calculated up to the incipient plastic flow are also reported). The ideal strength is assumed to be of 100GPa and the theoretical Young's modulus of 1,300 GPa; by (14.13) the crack length n is calculated and introduced in (14.19) to derive the related vacancy fraction v ($\xi = \pi/2$)

14.10 Thermodynamic Limit

Defects are thermodynamically unavoidable, especially at the macroscale. At the thermal equilibrium the vacancy fraction $f = n/N << 1$, n is the number of vacancies and N is here the total number of atoms, is estimated as [36]:

$$f \approx e^{-E_1/(k_B T_a)}, \tag{14.21}$$

where $E_1 \approx 7\,\text{eV}$ is the energy required to remove one carbon atom and T_a is the absolute temperature at which the carbon is assembled, typically in the range between 2,000 and 4,000 K. Thus, $f \approx 2.4 \times 10^{-18} - 1.6 \times 10^{-9}$.

The strength of a bundle will be dictated by the largest transversal crack on it, according to the weakest link concept. The probability of finding a nanocrack of size m in a bundle with vacancy fraction f is $P(m) = (1-f)\,f^m$, and thus the number M of such nanocracks in a bundle composed by N atoms is $M(m) = P(m)\,N$. The size of the largest nanocrack, which typically occurs

once, is found from the solution to the equation $M(m) \approx 1$, which implies [37]:

$$m \approx -\ln[(1-f)N] / \ln f \approx -\ln N / \ln f \tag{14.22}$$

Inserting (14.21) and (14.22) into (14.13) evaluated for a transversal crack ($b \approx 0$ and $2a / q \approx m$), we deduce the statistical counterpart of (14.13) and thus the following thermodynamical maximum achievable strength [38]:

$$\frac{\sigma_{\mathrm{N}}(N)}{\sigma_{\mathrm{N}}^{(\mathrm{theo})}} \leq \frac{\sigma_{\mathrm{N}}^{(\max)}(N)}{\sigma_{\mathrm{N}}^{(\mathrm{theo})}} = \frac{1}{\sqrt{1 + \frac{k_B T_a}{E_1} \ln N}} \tag{14.23}$$

14.11 Hierarchical Simulations and Size Effects: from a Nanotube to a Megacable

To evaluate the strength of carbon nanotube cables, the SE^3 algorithm, formerly proposed [39], has been adopted [40]. Multiscale simulations are necessary in order to tackle the size scales from a nanotube to a bundle. Let us consider the limit case of a nanotube based megacable, such as that of the space elevator [21, 38–40], Fig. 14.2.

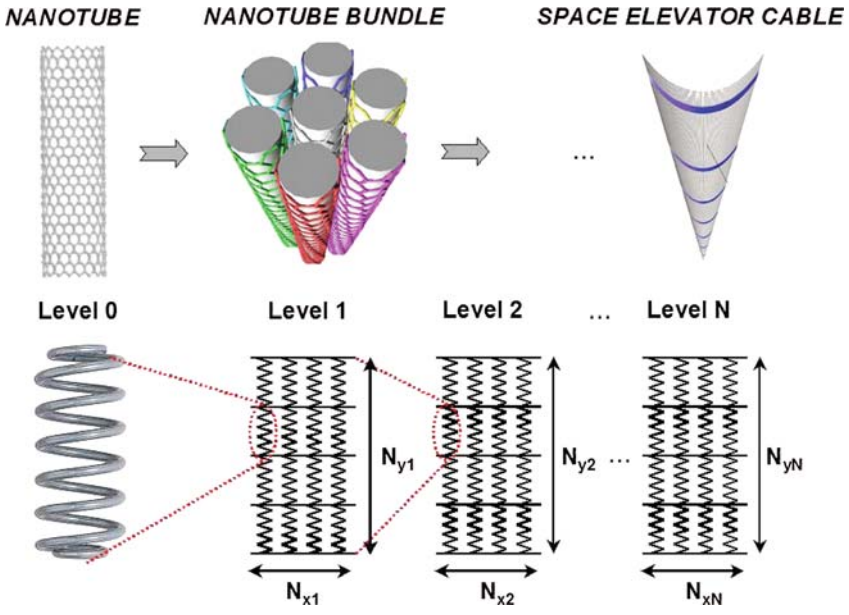

Fig. 14.2. Schematization of the adopted multiscale simulation procedure to determine the nanotube cable strength, from a nanotube to a megacable, here considered to be the limiting case of the space elevator cable. Here, $N = 5$, $N_{x1} = N_{x2} = \ldots N_{x5} = 40$ and $N_{y1} = N_{y2} = \ldots N_{y5} = 1,000$, so that the total number of nanotubes in the largest considered cable is $N_{\mathrm{tot}} = (1,000 \times 40)^5 \approx 10^{23}$

The bundle is modelled as an ensemble of stochastic "springs", arranged in parallel sections. Linearly increasing strains are applied to the fibre bundle, and at each algorithm iteration the number of fractured springs is computed (fracture occurs when local stress exceeds the nanotube failure strength) and the strain is uniformly redistributed among the remaining intact springs in each section.

In-silico stress-strain experiments have been carried out according to the following hierarchical architecture. Level 1: the nanotubes (single springs, Level 0) are considered with a given elastic modulus and failure strength distribution and composing a $40 \times 1,000$ lattice or fibre. Level 2: again a $40 \times 1,000$ lattice composed by second level "springs", each of them identical to the entire fibre analysed at the first level, is analysed with in input the elastic modulus and stochastic strength distribution derived as the output of the numerous simulations to be carried out at the first level. And so on. Five hierarchical levels are sufficient to reach the size-scale of the megametre from that of the nanometre, Fig. 14.2.

The level 1 simulation is carried out with springs $L_0 = 10^{-7}$m in length, $w_0 = 10^{-9}$m in width, with Young's modulus $E_0 = 10^{12}$Pa and strength σ_f randomly distributed according to NWS [34] fitting to experiments [4,5], thus assuming $\sigma_0 = 34\,\text{GPa}$ and $m = 2.7$. Then the level 2 is computed, and so on. The results are summarized in Fig. 14.3, in which a strong size effect is observed, up to length of $\sim$1 m.

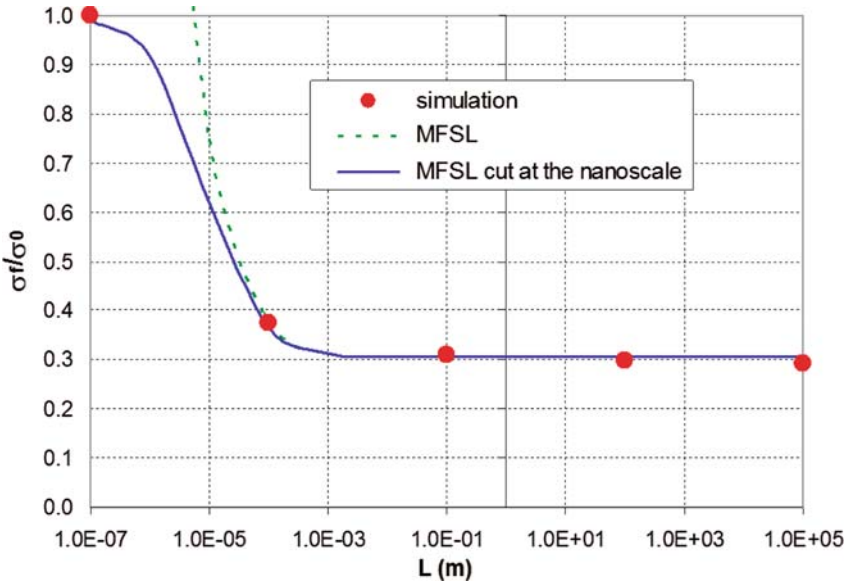

Fig. 14.3. Comparison between simulations and analytical scaling law, (14.24), for the failure strength of the nanotube bundle as a function of its length; the asymptote is at 10.20 GPa

Given the decaying σ_f vs. cable length L obtained from simulations, it is interesting to fit the behaviour with analytical scaling laws. Various exist in the literature, and one of the most used is the Multi Fractal Scaling Law (MFSL [41, 42]). This law has been recently extended towards the nanoscale [43], deriving (according to the theory of the geometrically necessary dislocations):

$$\frac{\sigma_f}{\sigma_{\text{macro}}} = \sqrt{1 + \frac{l_{\text{ch}}}{L + l_0}}, \tag{14.24}$$

where σ_f is the failure stress, σ_{macro} is the macrostrength, L is the structural characteristic size, l_{ch} is a characteristic internal length and l_0 is defined via $\sigma_f\,(l = 0) = \sigma_{\text{macro}}\sqrt{1 + \frac{l_{\text{ch}}}{l_0}} \equiv \sigma_{\text{nano}}$, where σ_{nano} is the nanostrength. Note that for $l_0 = 0$ this law is identical to the MFSL [41, 42]. Here, we can choose σ_{nano} as the nanotube stochastic strength, i.e. $\sigma_{\text{nano}} = 34\,\text{GPa}$. The computed macrostrength is $\sigma_{\text{macro}} = 10.20\,\text{GPa}$. The fit with (14.1) is shown in Fig. 14.3 ("MFSL cut at the nanoscale"), for the various L considered at the different hierarchical levels (and compared with the classical "MFSL"). The best fit is obtained for $l_{\text{ch}} = 5\times10^{-5}\,\text{m}$, where the analytical law is practically coincident with the simulated results. Thus, for a carbon nanotube bundle not shorter than a millimetre, the expected strength is $\sigma_{\text{C}} = \sigma_{\text{macro}} \approx 10 - 30\,\text{GPa}$, where the upper limit would correspond to assume a theoretical value of $\sigma_{\text{nano}} = 100\,\text{GPa}$.

14.12 Conclusions

The strength and fatigue life of a real, thus defective, carbon nanotube and bundle are expected to be strongly reduced with respect to their theoretical values. Less dramatic, but still significant, could be the reduction imposed by defects on their elasticity. Accordingly, we conclude that a proper and novel design of ultra-sharp tips based on CNT has to take into account the role of defects. QFM approaches are ideal to design flaw-tolerant nanomaterials and nanostructures, such as the discussed CNT tips for scanning probe "nanoscopy".

References

1. H. Dai, J.H. Hafner, A.G. Rinzler, D.T. Colbert, R.E. Smalley Nature **384** 147 (1996)
2. S.S. Wong, A.T. Woolley, T.W. Odom, J.L. Huang, P. Kim, D.V. Vezenov, C.M. Lieber Appl. Phys. Lett. **73** 3465 (1998)
3. C.V. Nguyen Q.i. Ye, M. Meyyappan Meas. Sci. Technol. **16** 2138 (2005)
4. M.F. Yu, B.S. Files, S. Arepalli, R. Ruoff Phys. Rev. Lett. **84** 5552 (2000)
5. M.F. Yu, O. Lourie, M.J. Dyer, K. Moloni, T.F. Kelly R. Ruoff Science **287** 637 (2000)

6. N. Pugno *A quantized Griffith's Criterion, Fracture Nanomechanics, Meeting of the Italian Group of Fracture* September 25–26, 2002, Vigevano, Italy
7. N. Pugno, R. Ruoff Philos. Mag. **84** 2829 (2004)
8. N. Pugno Int. J. Fract. **140** 158 (2006)
9. N. Pugno Int. J. Fract. **141** 311 (2006)
10. A.A. Griffith Phil. Trans. R. Soc. Lond. Biol. Sci **A221** 163 (1921)
11. L.B. Freund *Dynamic Fracture Mechanics* (Cambridge University Press, Cambridge, 1990)
12. H. Neuber *Theory of Notch Stresses* (Springer, Berlin, 1958)
13. V. Novozhilov Prik. Mat. Mek. **33** 212 (1969)
14. N.F. Morozov, V. Yu Petrov, A.A. Utkin Sov. Phys. Dokl. **35** 646 (1990)
15. P. Cornetti, N. Pugno, A. Carpinteri, D. Taylor Eng. Fract. Mech. **73** 2021 (2006)
16. D. Taylor, P. Cornetti, N. Pugno Eng. Fract. Mech. **72** 1021 (2005)
17. H. Murakami *Stress Intensity Factors Handbook* (Pergamon Press, Oxford, 1986)
18. N. Pugno, P. Cornetti, A. Carpinteri Eng. Fract. Mech. **74** 595 (2007)
19. N. Pugno, M. Ciavarella, P. Cornetti, A. Carpinteri J. Mech. Phys. Solids **54** 1333 (2006)
20. W. Weibull Handlingar, Nr 151 (1939)
21. N. Pugno Acta Mater. **55** 5269 (2007)
22. J.R. Rice, G.F. Rosengren J. Mech. Phys. Solids **16** 1 (1968)
23. A. Carpinteri, N. Pugno Eng. Fract. Mech. **72** 1254 (2005)
24. A. Carpinteri, B. Chiaia Int. J. Fract. **76** 327 (1996)
25. N. Pugno Appl. Phys. Lett. **90** 043106 (2007)
26. S.L. Mielke, D. Troya, S. Zhang, J.L. Li, S. Xiao, R. Car, R. Ruoff, S., G.C. Schatz, T. Belytschko Chem. Phys. Lett. **390** 413 (2004)
27. T. Belytschko, S.P. Xiao, R. Ruoff *Effects of defects on the strength of nanotubes: experimental-computational comparisons,* Los Alamos National Laboratory, Preprint Archive, Physics, arXiv:physics/0205090 (2002)
28. S. Zhang, S.L. Mielke, R. Khare, D. Troya, R.S. Ruoff, G.C. Schatz, T. Belytschko Phys. Rev. B **71** 115403 1 (2005)
29. R. Khare, S.L. Mielke, J.T. Paci, S. Zhang, R. Ballarini, G.C. Schatz, T. Belytschko Phys. Rev. B **75** 075412 (2007)
30. M. Ippolito, A. Mattoni, L. Colombo, N. Pugno Phys. Rev. B **73** 104111–1/6 (2006)
31. W. Ding, L. Calabri, K.M. Kohlhaas, X. Chen, D.A. Dikin, R.S. Ruoff Modulus Exp. Mech. **47** 25 (2006)
32. M. Meo, M. Rossi Eng. Fract. Mech. **73** 2589 (2006)
33. M. Sammalkorpi, A. Krasheninnikov, A. Kuronen, K. Nordlund, K. Kaski Phys. Rev. B **70** 245416–1/8 (2004)
34. N. Pugno, R. Ruoff J. Appl. Phys. **99** 1 (2006)
35. A.H. Barber, I. Kaplan-Ashiri, S.R. Cohen, R. Tenne, H.D. Wagner Compos. Sci. Technol. **65** 2380 (2005)
36. C. Kittel *Introduction to Solid State Physics* (Wiley, New York, 1966)
37. P.D. Beale, D.J. Srolovitz Phys. Rev. B **37** 5500 (1988)
38. N. Pugno Nano Today **2** 44 (2007)
39. N. Pugno J. Phys. Condens. Matter **18** S1971 (2006)
40. N. Pugno, F. Bosia, A. Carpinteri Small **4** 1044 (2008)
41. A. Carpinteri Int. J. Solid Struct. **31** 291 (1994)
42. A. Carpinteri Mech. Mater. **18** 89 (1994)
43. N. Pugno Acta Mater. **55** 1947 (2007)